Research Collection School Of Computing and Information Systems

School of Computing and Information Systems

8-1995

Limit on B0s oscillation using a jet charge method

D. BUSKULIC

M. THULASIDAS
Singapore Management University, manojt@smu.edu.sg

Citation

1

EUROPEAN LABORATORY FOR PARTICLE PHYSICS (CERN)

Limit on B_s^0 Oscillation Using a Jet Charge Method

The ALEPH Collaboration*

Abstract

A lower limit is set on the B_s^0 meson oscillation parameter Δm_s using data collected from 1991 to 1994 by the ALEPH detector. Events with a high transverse momentum lepton and a reconstructed secondary vertex are used. The high transverse momentum leptons are produced mainly by b hadron decays, and the sign of the lepton indicates the particle/antiparticle final state in decays of neutral B mesons. The initial state is determined by a jet charge technique using both sides of the event. A maximum likelihood method is used to set a lower limit of Δm_s. The 95% confidence level lower limit on Δm_s ranges between 5.2 and $6.5 (\hbar/c^2)$ ps^{-1} when the fraction of b quarks from Z^0 decays that form B_s^0 mesons is varied from 8% to 16%. Assuming that the B_s^0 fraction is 12%, the lower limit would be $\Delta m_s > 6.1 (\hbar/c^2)$ ps^{-1} at 95% confidence level. For $x_s = \Delta m_s \tau_{B_s}$, this limit also gives $x_s > 8.8$ using the B_s^0 lifetime of $\tau_{B_s} = 1.55 \pm 0.11$ ps and shifting the central value of τ_{B_s} down by 1σ.

*See the following pages for the list of authors.

The ALEPH Collaboration

D. Buskulic, D. Casper, I. De Bonis, D. Decamp, P. Ghez, C. Goy, J.-P. Lees, A. Lucotte, M.-N. Minard, P. Odier, B. Pietrzyk

Laboratoire de Physique des Particules (LAPP), IN^{2}P^3-CNRS, 74019 Annecy-le-Vieux Cedex, France

F. Ariztizabal, M. Chmeissani, J.M. Crespo, I. Efthymiopoulos, E. Fernandez, M. Fernandez-Bosman, V. Gaitan, Ll. Garrido,[15] M. Martinez, S. Orteu, A. Pacheco, C. Padilla, F. Palla, A. Pascual, J.A. Perlas, F. Sanchez, F. Teubert

Institut de Fisica d'Altes Energies, Universitat Autonoma de Barcelona, 08193 Bellaterra (Barcelona), Spain[7]

A. Colaleo, D. Creanza, M. de Palma, A. Farilla, G. Gelao, M. Girone, G. Iaselli, G. Maggi,[3] M. Maggi, N. Marinelli, S. Natali, S. Nuzzo, A. Ranieri, G. Raso, F. Romano, F. Ruggieri, G. Selvaggi, L. Silvestris, P. Tempesta, G. Zito

Dipartimento di Fisica, INFN Sezione di Bari, 70126 Bari, Italy

X. Huang, J. Lin, Q. Ouyang, T. Wang, Y. Xie, R. Xu, S. Xue, J. Zhang, L. Zhang, W. Zhao

Institute of High-Energy Physics, Academia Sinica, Beijing, The People's Republic of China[8]

G. Bonvicini, D.G. Cassel,[27] M. Cattaneo, P. Comas, P. Coyle, H. Drevermann, A. Engelhardt, R.W. Forty, M. Frank, R. Hagelberg, J. Harvey, R. Jacobsen,[24] P. Janot, B. Jost, J. Knobloch, I. Lehraus, C. Markou,[23] E.B. Martin, P. Mato, T. Mattison,[28] H. Meinhard, A. Minten, R. Miquel, K. Moffeit,[28] T. Oest, P. Palazzi, J.R. Pater,[29] J.-F. Pusztaszeri, F. Ranjard, P. Rensing, L. Rolandi, D. Schlatter, M. Schmelling, O. Schneider, W. Tejessy, I.R. Tomalin, A. Venturi, H. Wachsmuth, W. Wiedenmann, T. Wildish, W. Witzeling, J. Wotschack

European Laboratory for Particle Physics (CERN), 1211 Geneva 23, Switzerland

Z. Ajaltouni, M. Bardadin-Otwinowska,[2] A. Barres, C. Boyer, A. Falvard, P. Gay, C. Guicheney, P. Henrard, J. Jousset, B. Michel, S. Monteil, J-C. Montret, D. Pallin, P. Perret, F. Podlyski, J. Proriol, J.-M. Rossignol, F. Saadi

Laboratoire de Physique Corpusculaire, Université Blaise Pascal, IN^{2}P^3-CNRS, Clermont-Ferrand, 63177 Aubière, France

T. Fearnley, J.B. Hansen, J.D. Hansen, J.R. Hansen, P.H. Hansen, B.S. Nilsson

Niels Bohr Institute, 2100 Copenhagen, Denmark[9]

A. Kyriakis, E. Simopoulou, I. Siotis, A. Vayaki, K. Zachariadou

Nuclear Research Center Demokritos (NRCD), Athens, Greece

A. Blondel, G. Bonneaud, J.C. Brient, P. Bourdon, L. Passalacqua, A. Rouge, M. Rumpf, R. Tanaka, A. Valassi,[33] M. Verderi, H. Videau

Laboratoire de Physique Nucléaire et des Hautes Energies, Ecole Polytechnique, IN²P³-CNRS, 91128 Palaiseau Cedex, France

D.J. Candlin, M.I. Parsons

Department of Physics, University of Edinburgh, Edinburgh EH9 3JZ, United Kingdom[10]

E. Focardi, G. Parrini

Dipartimento di Fisica, Università di Firenze, INFN Sezione di Firenze, 50125 Firenze, Italy

M. Corden, M. Delfino,[12] C. Georgiopoulos, D.E. Jaffe

Supercomputer Computations Research Institute, Florida State University, Tallahassee, FL 32306-4052, USA [13,14]

A. Antonelli, G. Bencivenni, G. Bologna,[4] F. Bossi, P. Campana, G. Capon, V. Chiarella, G. Felici, P. Laurelli, G. Mannocchi,[5] F. Murtas, G.P. Murtas, M. Pepe-Altarelli

Laboratori Nazionali dell'INFN (LNF-INFN), 00044 Frascati, Italy

S.J. Dorris, A.W. Halley, I. ten Have,[6] I.G. Knowles, J.G. Lynch, W.T. Morton, V. O'Shea, C. Raine, P. Reeves, J.M. Scarr, K. Smith, M.G. Smith, A.S. Thompson, F. Thomson, S. Thorn, R.M. Turnbull

Department of Physics and Astronomy, University of Glasgow, Glasgow G12 8QQ,United Kingdom[10]

U. Becker, O. Braun, C. Geweniger, G. Graefe, P. Hanke, V. Hepp, E.E. Kluge, A. Putzer, B. Rensch, M. Schmidt, J. Sommer, H. Stenzel, K. Tittel, S. Werner, M. Wunsch

Institut für Hochenergiephysik, Universität Heidelberg, 69120 Heidelberg, Fed. Rep. of Germany[16]

R. Beuselinck, D.M. Binnie, W. Cameron, D.J. Colling, P.J. Dornan, N. Konstantinidis, L. Moneta, A. Moutoussi, J. Nash, G. San Martin, J.K. Sedgbeer, A.M. Stacey

Department of Physics, Imperial College, London SW7 2BZ, United Kingdom[10]

G. Dissertori, P. Girtler, E. Kneringer, D. Kuhn, G. Rudolph

Institut für Experimentalphysik, Universität Innsbruck, 6020 Innsbruck, Austria[18]

C.K. Bowdery, T.J. Brodbeck, P. Colrain, G. Crawford, A.J. Finch, F. Foster, G. Hughes, T. Sloan, E.P. Whelan, M.I. Williams

Department of Physics, University of Lancaster, Lancaster LA1 4YB, United Kingdom[10]

A. Galla, A.M. Greene, K. Kleinknecht, G. Quast, J. Raab, B. Renk, H.-G. Sander, R. Wanke, C. Zeitnitz

Institut für Physik, Universität Mainz, 55099 Mainz, Fed. Rep. of Germany[16]

J.J. Aubert, A.M. Bencheikh, C. Benchouk, A. Bonissent,[21] G. Bujosa, D. Calvet, J. Carr, C. Diaconu, F. Etienne, M. Thulasidas, D. Nicod, P. Payre, D. Rousseau, M. Talby

Centre de Physique des Particules, Faculté des Sciences de Luminy, IN²P³-CNRS, 13288 Marseille, France

I. Abt, R. Assmann, C. Bauer, W. Blum, D. Brown, H. Dietl, F. Dydak, G. Ganis, C. Gotzhein, K. Jakobs, H. Kroha, G. Lütjens, G. Lutz, W. Männer, H.-G. Moser, R. Richter, A. Rosado-Schlosser, A. Schwarz,[34] R. Settles, H. Seywerd, U. Stierlin,[2] R. St. Denis, G. Wolf

Max-Planck-Institut für Physik, Werner-Heisenberg-Institut, 80805 München, Fed. Rep. of Germany[16]

R. Alemany, J. Boucrot, O. Callot, A. Cordier, F. Courault, M. Davier, L. Duflot, J.-F. Grivaz, Ph. Heusse, M. Jacquet, D.W. Kim,[19] F. Le Diberder, J. Lefrançois, A.-M. Lutz, G. Musolino, I. Nikolic, H.J. Park, I.C. Park, M.-H. Schune, S. Simion, J.-J. Veillet, I. Videau

Laboratoire de l'Accélérateur Linéaire, Université de Paris-Sud, IN²P³-CNRS, 91405 Orsay Cedex, France

D. Abbaneo, P. Azzurri, G. Bagliesi, G. Batignani, S. Bettarini, C. Bozzi, G. Calderini, M. Carpinelli, M.A. Ciocci, V. Ciulli, R. Dell'Orso, R. Fantechi, I. Ferrante, L. Foà,[1] F. Forti, A. Giassi, M.A. Giorgi, A. Gregorio, F. Ligabue, A. Lusiani, P.S. Marrocchesi, A. Messineo, G. Rizzo, G. Sanguinetti, A. Sciabà, P. Spagnolo, J. Steinberger, R. Tenchini, G. Tonelli,[26] G. Triggiani, C. Vannini, P.G. Verdini, J. Walsh

Dipartimento di Fisica dell'Università, INFN Sezione di Pisa, e Scuola Normale Superiore, 56010 Pisa, Italy

A.P. Betteridge, G.A. Blair, L.M. Bryant, F. Cerutti, Y. Gao, M.G. Green, D.L. Johnson, T. Medcalf, Ll.M. Mir, P. Perrodo, J.A. Strong

Department of Physics, Royal Holloway & Bedford New College, University of London, Surrey TW20 OEX, United Kingdom[10]

V. Bertin, D.R. Botterill, R.W. Clifft, T.R. Edgecock, S. Haywood, M. Edwards, P. Maley, P.R. Norton, J.C. Thompson

Particle Physics Dept., Rutherford Appleton Laboratory, Chilton, Didcot, Oxon OX11 OQX, United Kingdom[10]

B. Bloch-Devaux, P. Colas, H. Duarte, S. Emery, W. Kozanecki, E. Lançon, M.C. Lemaire, E. Locci, B. Marx, P. Perez, J. Rander, J.-F. Renardy, A. Rosowsky, A. Roussarie, J.-P. Schuller, J. Schwindling, D. Si Mohand, A. Trabelsi, B. Vallage

CEA, DAPNIA/Service de Physique des Particules, CE-Saclay, 91191 Gif-sur-Yvette Cedex, France[17]

R.P. Johnson, H.Y. Kim, A.M. Litke, M.A. McNeil, G. Taylor

Institute for Particle Physics, University of California at Santa Cruz, Santa Cruz, CA 95064, USA[22]

A. Beddall, C.N. Booth, R. Boswell, S. Cartwright, F. Combley, I. Dawson, A. Koksal, M. Letho, W.M. Newton, C. Rankin, L.F. Thompson

Department of Physics, University of Sheffield, Sheffield S3 7RH, United Kingdom[10]

A. Böhrer, S. Brandt, G. Cowan, E. Feigl, C. Grupen, G. Lutters, J. Minguet-Rodriguez, F. Rivera,[25] P. Saraiva, L. Smolik, F. Stephan

Fachbereich Physik, Universität Siegen, 57068 Siegen, Fed. Rep. of Germany[16]

M. Apollonio, L. Bosisio, R. Della Marina, G. Giannini, B. Gobbo, F. Ragusa[20]

Dipartimento di Fisica, Università di Trieste e INFN Sezione di Trieste, 34127 Trieste, Italy

J. Rothberg, S. Wasserbaech

Experimental Elementary Particle Physics, University of Washington, WA 98195 Seattle, U.S.A.

S.R. Armstrong, L. Bellantoni,[32] P. Elmer, Z. Feng, D.P.S. Ferguson, Y.S. Gao, S. González, J. Grahl, J.L. Harton,[30] O.J. Hayes, H. Hu, P.A. McNamara III, J.M. Nachtman, W. Orejudos, Y.B. Pan, Y. Saadi, M. Schmitt, I.J. Scott, V. Sharma,[31] J.D. Turk, A.M. Walsh, Sau Lan Wu, X. Wu, J.M. Yamartino, M. Zheng, G. Zobernig

Department of Physics, University of Wisconsin, Madison, WI 53706, USA[11]

1   Introduction

Flavour non-conservation in charged weak current interactions allows particle/antiparticle oscillations in neutral B mesons [1]. Consider either the B_d^0 or the B_s^0 system. Let B^0 stand for either B_d^0 or B_s^0, and $\overline{B}^0$ for either $\overline{B}_d^0$ or $\overline{B}_s^0$. If CP non-invariance is neglected, then the probability distribution for a meson which is created as B^0 (or $\overline{B}^0$) to decay as a B^0 (or $\overline{B}^0$) after a proper time t is

$$\mathcal{P}_u(t) = \frac{\Gamma}{2}e^{-\Gamma t}(1 + \cos \Delta m t), \tag{1}$$

where the subscript u denotes "unmixed," Δm is the mass difference between the mass eigenstates, and Γ is the decay rate, which is taken to be the same for both states. (The convention $\hbar = c = 1$ is used throughout this paper.) Similarly, the probability distribution for a B^0 (or $\overline{B}^0$) to decay as its antiparticle after a proper time t is

$$\mathcal{P}_m(t) = \frac{\Gamma}{2}e^{-\Gamma t}(1 - \cos \Delta m t), \tag{2}$$

where the subscript m stands for "mixed."

In the Standard Model, the processes governing B_s^0 and B_d^0 oscillations are nearly the same except for the different masses and the different CKM [2] matrix elements V_{ts} and V_{td}. Most of the theoretical uncertainty cancels if mixing in the two systems [1] is compared:

$$\frac{\Delta m_s}{\Delta m_d} = \frac{m_{B_s}}{m_{B_d}} \left| \frac{V_{ts}}{V_{td}} \right|^2 \xi_s^2 \frac{\hat{\eta}_{B_s}}{\hat{\eta}_{B_d}}, \tag{3}$$

where $\hat{\eta}_{B_s}$ and $\hat{\eta}_{B_d}$ are the QCD correction factors for the B_s^0 and B_d^0, expected to be similar, and ξ_s is the ratio of hadronic matrix elements for the B_s^0 and B_d^0. Estimates from lattice QCD [3] and QCD sum rules [4] are consistent with a value of $\xi_s = 1.16 \pm 0.10$ [5].

For the B_d^0 system, time-dependent mixing has been observed by the ALEPH, OPAL and DELPHI Collaborations at LEP [6, 7, 8, 9, 10, 11]. For the B_s^0 system, 95% confidence lower limits of $\Delta m_s > 1.8\,\mathrm{ps}^{-1}$ [7] and $\Delta m_s > 2.2\,\mathrm{ps}^{-1}$ [11] have been set by ALEPH and OPAL respectively. These limits were obtained using events where both b hadrons decay semileptonically.

This paper describes an investigation of time-dependent B_s^0-$\overline{B}_s^0$ mixing using the ALEPH data. Events are selected from hadronic Z decays containing at least one high p_T lepton. There is a significant increase in the event sample by using jet charge in the event, instead of relying on another high p_T lepton in the opposite hemisphere, to determine the initial quark state. In $Z \to b\bar{b}$ events where $b \to c\,\ell^-\,\bar{\nu}$, the charge of the lepton has the same sign as that of the b quark at decay. Hence the particle/antiparticle state at the time the B^0 decays is determined by the sign of the lepton charge. The determination of the particle/antiparticle state of the B^0 at production is achieved by a rapidity weighted jet charge technique [12] using information from both sides of the event. In the determination of Δm_s, the method of maximum likelihood is used to study the fractions of mixed and unmixed events as a function of the reconstructed proper times of the B_s^0 mesons which undergo semileptonic decays.

2 Event Selection

This analysis is based on approximately 3.4 million hadronic Z^0 decays collected in the ALEPH experiment during the 1991–1994 data runs.

A detailed description of the ALEPH detector [13] and its performance [14] are available elsewhere. The vertex detector (VDET) consists of two layers of double-sided silicon microstrip detectors. The inner layer is at an average radius of 6.5 cm from the beam axis, and covers 85% of the solid angle. The outer layer is at 11.3 cm, and covers 69% of the solid angle. The point resolution at normal incidence is 12 μm in both the z and $r\phi$ projections. Charged tracks are then measured in an inner tracking chamber (ITC) of outer radius 26 cm, followed by a time projection chamber (TPC) from 40 to 171 cm in radius. The momentum resolution for charged tracks combining VDET, ITC and TPC information in the 1.5 T magnetic field is $\sigma_p/p = 0.0006p$ GeV^{-1} for high momentum tracks. The TPC also provides up to 338 measurements of specific ionization dE/dx which allows 3σ e/π separation for particle momenta up to 8 GeV. The electromagnetic calorimeter (ECAL), situated within the superconducting solenoidal magnet, is used with the TPC to identify electrons. The ECAL energy resolution is $\sigma_E/E = 0.18/\sqrt{E}$ (E in GeV). The hadronic calorimeter (HCAL) and the muon chambers surrounding it are used to identify muons. The total thickness of the calorimeter system is more than 8 interaction lengths.

A Monte Carlo sample of 2.0 million fully simulated hadronic events is used in this study. The Monte Carlo generator is based on JETSET 7.3 [15] with updated branching ratios. The Körner-Schuler model [16] is used for semileptonic b decays. A fast Monte Carlo based on the distributions in the fully simulated Monte Carlo is also used in Section 7 for setting the limit on Δm_s.

To select hadronic events, at least five tracks are required which satisfy the following criteria: $|\cos\theta| < 0.95$ (with respect to the beam axis), approaching within 2.0 cm of the beam axis, and within 10.0 cm of the interaction point in z at the nearest approach to the beam axis, having ≥ 4 TPC hits, and momentum $p < 45$ GeV. The momentum sum of these tracks must exceed 10% of the LEP beam energy. In each event the charged and neutral particles (determined by an energy-flow algorithm [14]) are separated into jets using the scaled-invariant-mass technique [17] with the y_c parameter set at 0.02. The event is required to have the thrust axis away from the beam axis ($|\cos\theta_{thrust}| < 0.85$). Events are then searched for leptons. If an event has one or more tracks satisfying the standard ALEPH selection criteria for leptons [18], the highest momentum lepton candidate is selected. Identified electrons and muons are required to have momentum greater than 2.0 and 3.0 GeV, respectively. The highest momentum lepton more than 90° away from the first is also selected if such a lepton is found. The leptons are associated with their nearest jets. These jets are also required to be separated by more than 90°. If only one lepton is found, the jet forming the highest invariant mass with the jet closest to the lepton is selected as the opposite side jet.

The transverse momentum p_T of the lepton from its associated jet is calculated with

the lepton momentum first subtracted from that of the jet. At least one lepton is required to have $p_T > 1.0$ GeV. These leptons are mainly produced by b hadrons, as they have sufficient mass to produce the large transverse momentum. The b hadron source fraction of the leptons is further enhanced by looking for evidence of a displaced b hadron decay vertex in the opposite hemisphere, where the hemispheres are defined by the thrust axis of the event. The method used in this analysis for separating a displaced heavy meson decay vertex from the interaction point yields a b–tagging variable in each hemisphere which is used to discriminate against light quark background contamination. The variable is the largest difference in χ^2 when some of the tracks in the hemisphere are assigned to a secondary vertex, compared to the case where all of the tracks in the hemisphere are assigned to the primary vertex. The χ^2 difference is required to be greater than 4.0 in the opposite hemisphere. This requirement removes 63% of the light quark background, and 46% of the charm quark background, while leaving 82% of the b quark events. The χ^2 calculation is explained in more detail in the next section.

3   Measurement of Decay Length and Momentum

The interaction point and decay vertex position must be reconstructed to determine the decay length of the b hadron. Tracking information from charged tracks in 75 successive hadronic events is used in a common fit to estimate the beam position and size in the $r\phi$ projection. The beam position can be measured to $30\,\mu$m in x and $10\,\mu$m in y. The typical rms of the spot size is $150\,\mu$m in x and $10\,\mu$m in y. The primary vertex position is reconstructed as follows: A coarse z coordinate is found using tracks which pass within 3 mm of the nominal beam axis. Tracks which have at least 4 TPC hits, χ^2 per degree of freedom less than 4, and which pass within 3 mm from the beam axis at a position in z which is within 3 mm of the coarse z coordinate are extrapolated into the plane defined by the measured y position of the beam. The y position of the beam is known to $10\,\mu$m, and is used as the y coordinate of the primary vertex. Grid points are spaced $20\,\mu$m apart in both x and z on this plane, and serve as candidate primary vertex positions. The χ^2 for each candidate vertex position is calculated using the impact points and errors of all tracks within 3σ of the candidate vertex point. The beam position and size in the x coordinate are also used in the χ^2 calculation. A paraboloid is fit to the χ^2 values of the grid points to interpolate the best primary vertex position. The curvature of the paraboloid gives the vertex error. The resolution in b hadron events is typically $90\,\mu$m along the flight direction.

Charged tracks which are in the same hemisphere as the high p_T lepton (excluding the lepton itself) are assigned to either the interaction point or a single reconstructed displaced decay vertex. Tracks are required to pass within 3 mm of the primary vertex (or 3 mm in r-ϕ if the z position error exceeds 1 mm near the primary vertex), have at least 4 TPC hits, and have χ^2 per degree of freedom less than 4. A three dimensional grid point search is performed for the secondary vertex position to find the displaced vertex

3

Fraction	Sigma (mm)	Offset (mm)
0.50	0.26	0.06
0.36	0.85	0.01
0.14	3.33	−0.79

Table 1: Parameters of the three Gaussian fit to the decay length resolution.

point–track assignment combination that has the greatest difference in χ^2 when compared to the case where all tracks are assumed to come from the interaction point. Tracks are required to come within 3σ of the vertex to be assigned to it. In addition, a 'jet-track' is defined by the primary vertex position and its errors, and parallel to the jet direction. It is given an additional angle error of 50 mrad, which is approximately the jet angular resolution. The jet-track information is included in the χ^2 calculations.

Tracks within 1.7σ of the displaced vertex point are combined to form a reconstructed charm track. If only one track passes this condition, it serves as the charm track. At least one of the tracks in the charm vertex is required to have a vertex detector hit. The charm track is then intersected with the lepton to form a candidate B_s^0 decay vertex. The lepton is required to have at least one vertex detector hit. The χ^2 for the reconstructed B vertex is required to be less than 10. The reconstructed decay length l is the projected distance from the production point to the b decay vertex along the jet direction. The Monte Carlo decay length resolution is shown in Fig 1(a). It is parameterized with the three offset Gaussians of Table 1. This parameterization is used in the fitting function of Section 5. As is shown in Fig 1(b), the resolution varies only slightly with true decay length. While this variation is not included in the fitting function, it is taken into account in the procedure used to set the limit on Δm_s (see Section 7).

The Monte Carlo parameterization of decay length resolution is checked in the data. Events are selected with the b–tagging variable in the opposite hemisphere less than 2.0 to enhance the uds fraction. The fraction of uds events in the fully simulated Monte Carlo sample is 80%. High transverse momentum tracks with the same kinematic properties as the leptons selected above are selected, except that these tracks are lepton *anti*-selected. Otherwise, the decay length reconstruction is the same as outlined above, with the "fake" lepton track serving as the lepton. Since most of these events are without tracks from secondary decay vertices, the decay length resolution can be determined by comparing the reconstructed decay points to the primary vertex. A comparison between data and Monte Carlo for these events indicates that the decay length resolution is underestimated by $\sim 10\%$ in the Monte Carlo. For this reason, the resolution used in subsequent sections is degraded by a scale factor of $S_{res} = 1.10$ with respect to that of the Monte Carlo.

The momentum of the b hadron must be estimated in order to calculate the proper time between its production and decay. The method used in this analysis has been
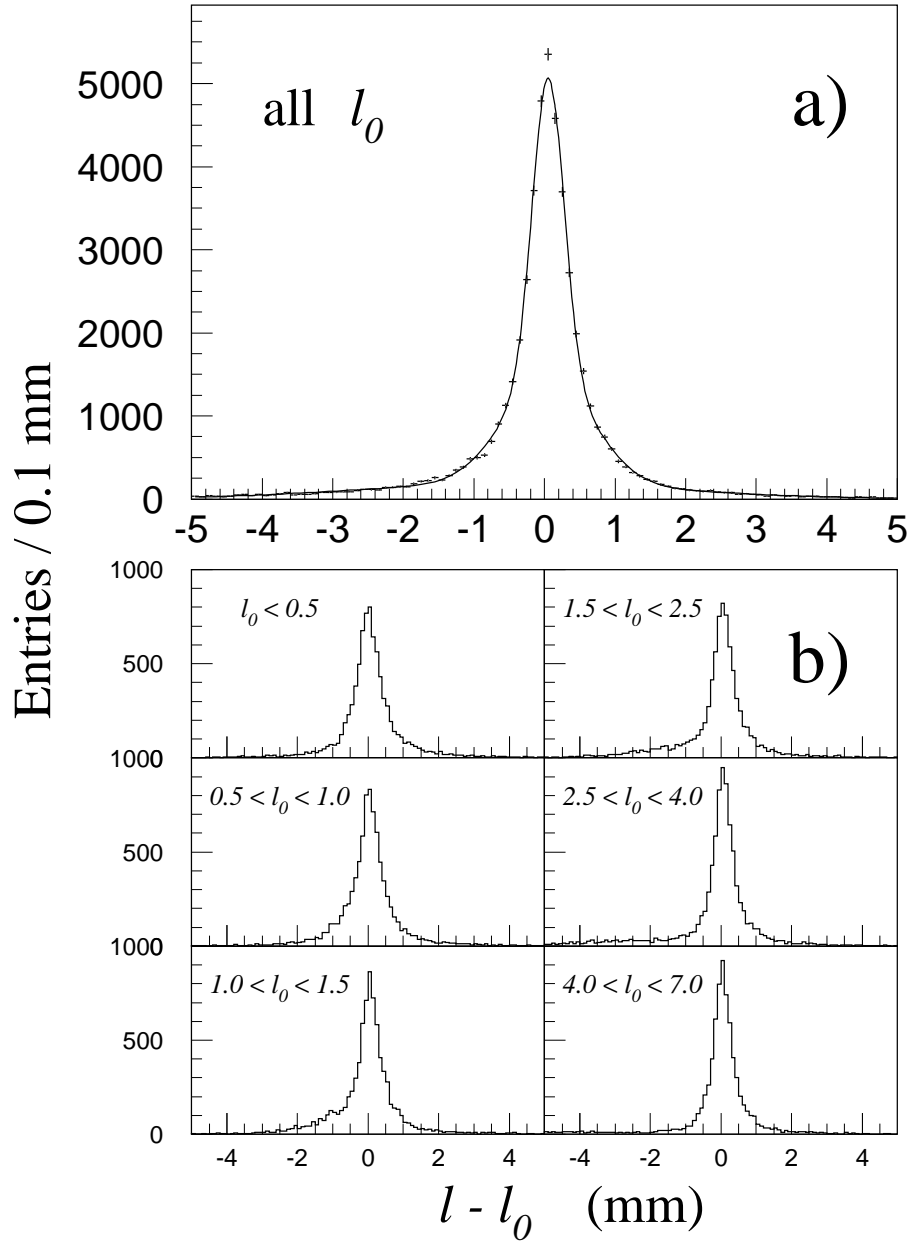
4

Figure 1: a) The Monte Carlo decay length resolution over the entire range of l_0 is fitted with three Gaussians, and the parameters from the fit are listed in Table 1. b) The resolution is also plotted in intervals of true decay length l_0 (in mm).

Fraction	Sigma (ps/cm)	Offset (ps/cm)
0.34	0.35	-0.05
0.46	1.1	0.00
0.20	3.5	-0.09

Table 2: Parameters for the three Gaussian fit to the g parameter.

described in the ALEPH dilepton mixing analysis [7]. The b hadron momentum is the sum of the lepton momentum, the momentum of the charged tracks assigned to the charm vertex, the estimated neutrino momentum, and a fraction of the measured jet momentum due to the energy of neutral particles measured in the calorimeter system. The neutrino energy is estimated as the difference between the beam energy and the amount of visible energy [14] in the hemisphere containing the lepton. The b hadron is assigned its average contribution of 67% of the measured momentum of neutral particles in the jet. This fraction is taken from the fully simulated Monte Carlo.

A term related to the true relativistic boost is defined as

$$g_0 = \frac{m_0}{p_0}, \tag{4}$$

where m_0 is the true mass of the appropriate b hadron, and p_0 is its true momentum. The true proper time in terms of the true decay distance l_0 is then

$$t_0 = g_0 \, l_0. \tag{5}$$

The reconstructed counterpart of g_0 is parameterized in terms of the reconstructed momentum:

$$g = \frac{m_b}{p}, \tag{6}$$

where m_b is an average b hadron mass of 5.3 GeV. The resolution in g is plotted in Fig 2, and the parameters of the three Gaussian fit are listed in Table 2. The core Gaussian corresponds to a relative resolution of $\sim 6\%$.

The reconstructed proper time is defined as:

$$t = g \, l. \tag{7}$$

The proper time resolution is plotted in Fig 3 in intervals of true proper time. The proper time resolution is not an input to the fitting function; a convolution of the resolutions in g and l (using the expected g and l distributions) is used instead. The result is superimposed for each of the intervals in Fig 3.
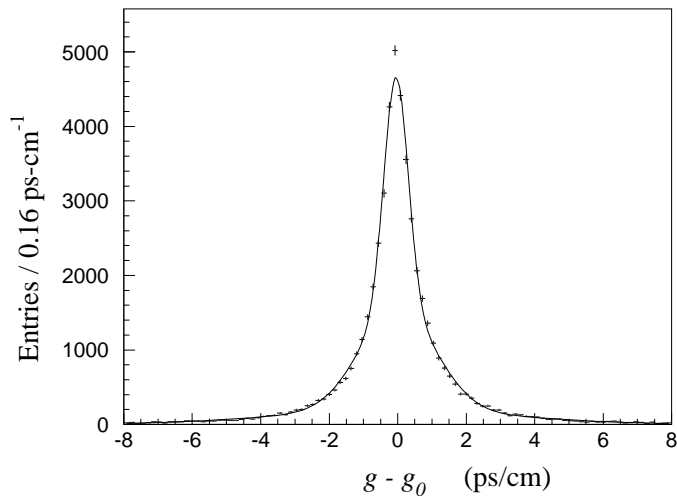
6

Figure 2: The resolution for the parameter g, as estimated in the full Monte Carlo simulation.

4 Determination of Particle/Antiparticle State at Production and Decay

To determine whether a B^0 meson has undergone mixing, it is necessary to determine the particle/antiparticle state of the meson at production time and when it decays. The final state is determined by the sign of the charge of the lepton tagging the b decay. The initial state is determined by measuring the residual charges of the two b quarks from the original $Z \rightarrow b\bar{b}$ decay, where the two quarks generally form jets in opposite hemispheres. The hemisphere of the b quark usually has negative net charge, while the opposite hemisphere has a positive charge corresponding to a $\bar{b}$ quark. A jet charge technique applied to both sides of the event has been used for measuring B_d^0 oscillations by OPAL [8], using momentum weighted charge. The present analysis instead uses a rapidity weighted jet charge defined as

$$Q_{jet} = \frac{\sum_{i=1}^{n} y_i q_i}{\sum_{i=1}^{n} y_i}, \tag{8}$$

where y_i is the rapidity defined as

$$y_i = \frac{1}{2} \log \frac{E_i + p_{i\|}}{E_i - p_{i\|}}, \tag{9}$$

and q_i is the charge of track i, E_i its energy, and $p_{i\|}$ its momentum component along the jet axis. The jet charges of both sides of the event are used to determine the state (B^0
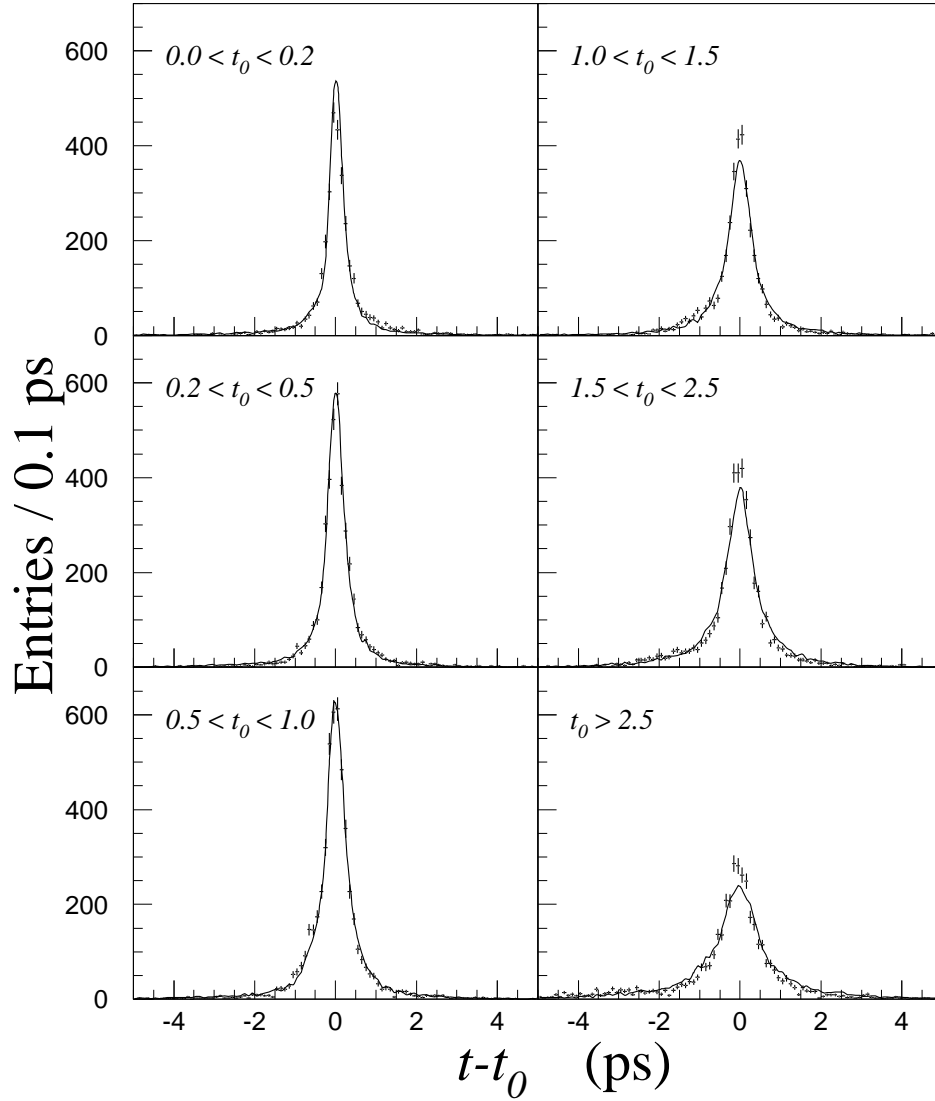
7

Figure 3: The Monte Carlo proper time resolution is plotted in intervals of true proper time t_0 (in ps). The superimposed curves are the expected distributions using the convolution of the parameterized g and l resolutions.

or $\overline{B}^0$) at production time of the jet containing the high p_T lepton. (The lepton charge is included in the jet charge calculation.)

A powerful variable to tag mixed or unmixed events is the lepton signed jet charge difference $q_\ell\,(Q_s - Q_o)$, where Q_s is the jet charge value for the jet in the same hemisphere as the lepton, Q_o is the jet charge value for the jet in the opposite hemisphere, and q_ℓ is the lepton charge. Fig 4(a) and (b) show that $q_\ell\,(Q_s - Q_o)$ is on average negative for mixed and positive for unmixed events. Fig 4(c) shows that Monte Carlo and data distributions in $q_\ell\,(Q_s - Q_o)$ agree well. Events with $q_\ell\,(Q_s - Q_o) > 0.2$ are tagged unmixed, while those with $q_\ell\,(Q_s - Q_o) < -0.2$ are tagged mixed. With this selection, 60% of truly mixed events have their mixed/unmixed state correctly determined, and 79% of unmixed events are correctly determined. The efficiency for the requirement of $|Q_s - Q_o| > 0.2$ is approximately 50%. Note that the 'tag rates' include effects of wrong–signed leptons when the lepton does not come directly from a semileptonic b decay, mostly due to semileptonic decays of the charm daughters of b hadrons. The total number of selected decays in the *tagged* mixed and unmixed ALEPH data samples are 10561 and 32856 respectively.

5   The Fitting Function

An unbinned maximum likelihood function is constructed for fitting the proper time distributions of mixed and unmixed events. $\mathcal{P}_g(g|g_0)$ and $\mathcal{P}_l(l|l_0)$ are (largely independent) conditional probability distributions: $\mathcal{P}_g(g|g_0)$ is the probability distribution of the measured value of g for a given value of true g_0, and $\mathcal{P}_l(l|l_0)$ is similarly defined. $\mathcal{P}_l(l|l_0)$ is taken as the sum of the three Gaussians of Table 1, and $\mathcal{P}_g(g|g_0)$ is given by the sum of the three Gaussians of Table 2.

The momentum distribution $D_0(p_0)$ of the B meson is taken to be of the Peterson form [19]. A change of variable from p_0 to g_0 then gives the joint distribution in g_0 and l_0 as

$$D(g_0, l_0) = \begin{cases} \frac{m_b}{\tau_b} \frac{1}{g_0} D_o\left(\frac{m_b}{g_0}\right) e^{-\frac{g_0 l_0}{\tau_b}} & \text{for } g_0 > \frac{m_b}{E_{beam}} \text{ and } l_0 > 0 \\ \\ 0 & \text{otherwise.} \end{cases} \tag{10}$$

With this $D(g_0, l_0)$, the joint distribution in g_0, l_0, g and l is then

$$\mathcal{P}(g_0, l_0, g, l) = D(g_0, l_0)\mathcal{P}_g(g|g_0)\mathcal{P}_l(l|l_0). \tag{11}$$

The fitted parameters are:

Δm_d, the mixing parameter for B_d^0 mesons;

A_u, the fraction of unmixed events correctly tagged as unmixed.
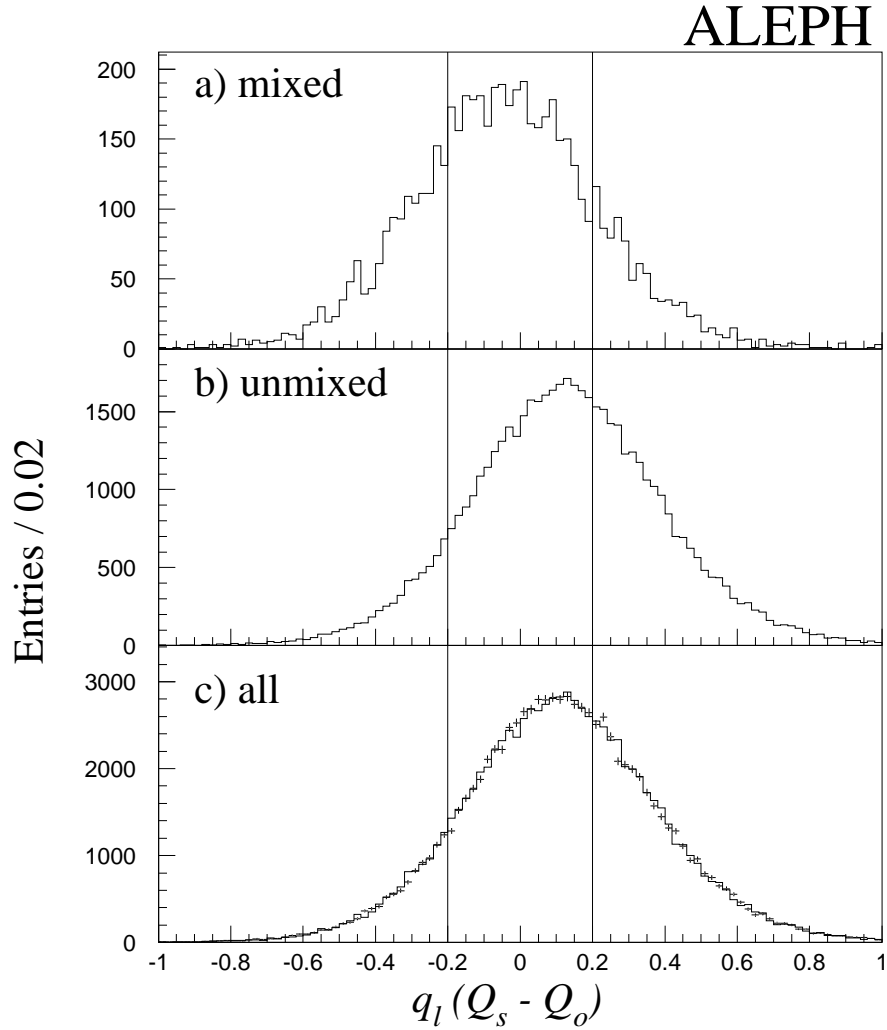
9

Figure 4: Lepton signed same side minus opposite side jet charge distributions for a) mixed B^0 mesons, and b) unmixed b hadrons in the full Monte Carlo simulation. Plotted in c) is the sum of all Monte Carlo events, normalized to the number of events in the data. The data points are superimposed with error bars. The vertical lines indicate the selection requirement $|Q_s - Q_o| > 0.2$.

The following variables are also used:

f_{B_s} is the fraction of b quarks which form B_s^0 mesons (weighted by the ratio of the B_s^0 semileptonic branching fraction to the average b hadron semileptonic branching fraction);

f_{B_d} is the fraction of b quarks which form B_d^0 mesons (weighted by the ratio of the B_d^0 semileptonic branching fraction to the average b hadron semileptonic branching fraction);

$\mathcal{E}_{B_s}$ is the reconstruction efficiency of B_s^0 mesons relative to $B^{\pm}$ and Λ_b hadrons;

$\mathcal{E}_{B_d}$ is the reconstruction efficiency of B_d^0 mesons relative to $B^{\pm}$ and Λ_b hadrons;

f_{uds} is the uds fraction of the selected event sample;

$f_{c\bar{c}}$ is the $c\bar{c}$ fraction of the selected event sample;

$f_{b\bar{b}} \equiv 1 - f_{c\bar{c}} - f_{uds}$;

A_m is the fraction of mixed events correctly tagged as mixed.

With the method of jet charge described above, the two tag rates A_u and A_m are different in value. The lifetimes τ_b of the various b hadrons are assumed equal for simplicity. The relative efficiencies for B_s^0 and B_d^0 mesons compared to other b hadrons are found to be $\mathcal{E}_{B_s} = 0.88$ and $\mathcal{E}_{B_d} = 0.90$. The loss in efficiency is mostly due to the jet charge cut which has a lower efficiency for mixed events. The fraction F_{B_s} of events with B_s^0 mesons with respect to all events is then

$$F_{B_s} = f_{b\bar{b}} \frac{\mathcal{E}_{B_s} f_{B_s}}{\mathcal{E}_{B_s} f_{B_s} + \mathcal{E}_{B_d} f_{B_d} + (1 - f_{B_s} - f_{B_d})}, \tag{12}$$

and similarly for F_{B_d}.

The probability distribution $\mathcal{P}(g_0, l_0, g, l)$ of equation (11) is used to get the desired mixed and unmixed distributions by:

$$\beta_m(g, l) = \int_0^{\infty} dg_0 \int_0^{\infty} dl_0 \ \alpha_m(g_0 l_0) \mathcal{P}(g_0, l_0, g, l), \tag{13}$$

and

$$\beta_u(g, l) = \int_0^{\infty} dg_0 \int_0^{\infty} dl_0 \ [1 - \alpha_m(g_0 l_0)] \mathcal{P}(g_0, l_0, g, l), \tag{14}$$

where

$$\alpha_m(t) = \frac{1}{2} F_{B_s}(1 - \cos \Delta m_s t) + \frac{1}{2} F_{B_d}(1 - \cos \Delta m_d t). \tag{15}$$

The non-b hadron (charm and uds) background events are treated as unmixed b hadrons, except that they have a different reconstructed proper time distribution. This

11

event type	lepton source	fraction (%)	sum (%)
B_s^0	$b \to \ell$	8.1	9.5
	$b \to c \to \ell$	0.7	
	$b \to$ other $\to \ell$	0.4	
	fake	0.3	
B_d^0	$b \to \ell$	26.8	33.2
	$b \to c \to \ell$	4.4	
	$b \to$ other $\to \ell$	1.2	
	fake	0.8	
other b hadron	$b \to \ell$	38.1	45.1
	$b \to c \to \ell$	3.9	
	$b \to$ other $\to \ell$	1.7	
	fake	1.4	
$c\bar{c}$	$c \to \ell$	8.2	9.2
	fake	1.0	
uds	$uds \to \ell$	0.6	3.0
	fake	2.4	

Table 3: Composition of the high p_T lepton sample in the fully simulated Monte Carlo. Misidentified hadrons are referred to as fakes.

proper time distribution is estimated from the fully simulated Monte Carlo sample and fitted with two exponentials convoluted with the resolution.

Finally, if N_m (N_u) is the number of events where the method of jet charge gives the result that the event is mixed (unmixed), then the likelihood function is given by

$$L = \prod_{i=1}^{N_m} [A_m \beta_m(g_i, l_i) + (1 - A_u)\beta_u(g_i, l_i)] \prod_{j=1}^{N_u} [(1 - A_m)\beta_m(g_j, l_j) + A_u \beta_u(g_j, l_j)]. \quad (16)$$

6 Studies of B_d^0 and B_s^0 Oscillations

The relative composition of the different sources of high p_T leptons in the event sample is estimated from the fully simulated Monte Carlo and shown in Table 3. These numbers depend on the input values to the full simulation: The fraction f_{B_s} of B_s^0 mesons produced out of all b hadrons generated is 12%, and the corresponding fraction for B_d^0 mesons is $f_{B_d} = 40\%$. The common lifetime τ_b for all b hadrons is 1.5 ps, and the mixing parameters for the B_s^0 and B_d^0 mesons are $\Delta m_s = 1.6$ ps^{-1} and $\Delta m_d = 0.467$ ps^{-1}, respectively.

A fit to the proper time distribution of the selected events yields a fraction of 7.6% of the events in the data sample which are compatible with having zero lifetime. Studies
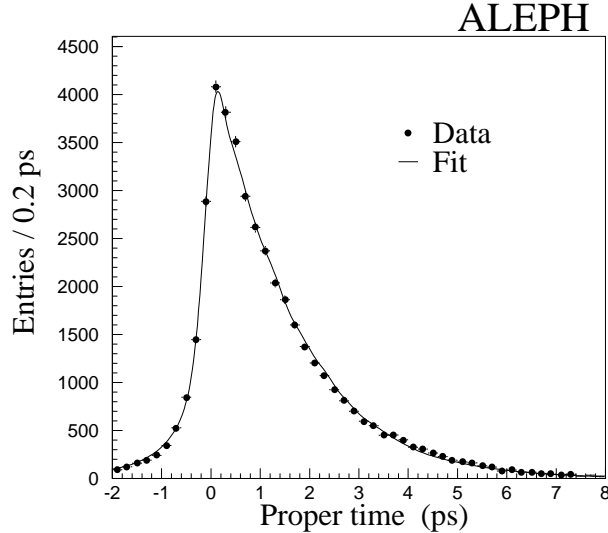
Figure 5: The proper time distribution for the data is plotted with the result of the lifetime fit superimposed.

of the composition of high p_T leptons in the ALEPH data suggest a *uds* fraction of $f_{uds} \approx 5.1\%$.[1] The remaining events, with fraction f_{sb}, belong to a class of *b* hadron events where the decay vertex is reconstructed near the primary vertex independent of the true *b* decay length. This happens mainly when there are few charged tracks from the true charm vertex, so a secondary vertex is reconstructed using tracks which are really from the primary vertex.

A correction is applied for decay length dependent efficiency found in the fully simulated Monte Carlo (mainly due to the χ^2 requirement on the reconstructed *b* vertex). The effect is treated by weighting events at longer decay lengths appropriately to account for the loss in efficiency, which is only significant for events at large decay length ($l > 1$ cm), and affects only about 3% of selected events. As a cross-check, a fit for the lifetime is performed. The fit in the data yields $\tau_b = 1.60 \pm 0.01$ ps and $\tau_b = 1.52 \pm 0.01$ ps for the Monte Carlo with 1.5 ps input lifetime. The errors are statistical only. The systematic error for the data is estimated to be about ± 0.07 ps, making the result compatible with the world average [20] of $\tau_b = 1.54 \pm 0.02$ ps. The reconstructed proper time distribution for the data is plotted in Fig 5 with the result of the lifetime fit superimposed.

The B_d^0 oscillation parameter Δm_d is determined as a check on the analysis. Assuming $\tau_b = 1.5$ ps, $f_{B_s} = 0.12$, $f_{B_d} = 0.40$, $\Delta m_s = 30$ ps^{-1}, and $A_m = 0.60$, a two-dimensional

---

[1]Note that this measured *uds* fraction is larger than the 3.0% found in the fully simulated Monte Carlo.

fit with the ALEPH data is performed for Δm_d and A_u. This gives $A_u = 0.792 \pm 0.003$ and $\Delta m_d = 0.47 \pm 0.04$ ps^{-1}, where the errors are statistical only. The value for Δm_d agrees with the world average [21] of 0.48 ± 0.03 ps^{-1}.

The Δm_s value used in the fit for the Monte Carlo is set at the input value of 1.6 ps^{-1}. The fit for the Monte Carlo yields $A_u = 0.790 \pm 0.004$ and $\Delta m_d = 0.48 \pm 0.05$ ps^{-1}, which agree with the input values of $A_u = 0.790$ and $\Delta m_d = 0.467$ ps^{-1}. Fig 6 shows the tagged mixed fraction for Monte Carlo and data. The solid curve for the fully simulated Monte Carlo is the expected distribution with the input value of $\Delta m_s = 1.6$ ps^{-1}. The solid curve for the data is the expected distribution for $\Delta m_s = 30$ ps^{-1}, while the dashed curve is the distribution for $\Delta m_s = 6$ ps^{-1}. Note that the sensitivity of this analysis comes from the unbinned maximum likelihood fit, not from a direct fit to the binned data as shown in the figure.

7   Setting the Limit for Δm_s and Studies of Systematic Effects

Fig 7(a) shows the $\Delta \log L$ curve for the data as a function of Δm_s, where $\Delta \log L$ is defined as the negative log likelihood value $(- \log L)$ at a given Δm_s minus the $- \log L$ value calculated at the Δm_s where the $- \log L$ is at its minimum. It uses the values of A_u and Δm_d determined above as inputs to the fit, and assumes a B_s^0 fraction of $f_{B_s} = 12\%$. The data prefer high values of Δm_s, with a favoured value of 8 ps^{-1}. The difference in likelihood for higher values of Δm_s is insufficient to exclude them, however, so a lower limit is therefore set on Δm_s. Superimposed on the data is a 95% confidence level lower limit curve calculated using a 'fast' Monte Carlo. The construction of the limit curve is discussed after the following description of the fast Monte Carlo simulation.

The fast Monte Carlo is intended to produce results similar to those found in the fully simulated Monte Carlo, while allowing greater freedom to study statistical and systematic effects. The input tag rates to the fast Monte Carlo are listed in Table 4. These are taken from the fully simulated Monte Carlo, and the errors are the statistical fluctuations corresponding to the size of the ALEPH data sample. The important parameters in the fully simulated Monte Carlo which are not accurately known are treated by generating fast Monte Carlo samples with their uncertainties included. For every generated sample, the parameters in Table 5 are selected from Gaussian distributions around their central values according to their uncertainties. The effects of the uncertainties are then included, as the data and fast Monte Carlo samples are analyzed with the same fitting function.

Event generation proceeds as follows: Constraining $f_{b\bar{b}} \equiv 1 - f_{c\bar{c}} - f_{uds}$, the overall flavour of the event is generated. The central value of $f_{c\bar{c}} = 0.09$ is taken from the fully simulated Monte Carlo, and $f_{uds} = 0.05$ as discussed in Section 6. For the $b\bar{b}$ events, the fraction f_{B_s} is fixed at 12% (the dependence of the limit on f_{B_s} is treated
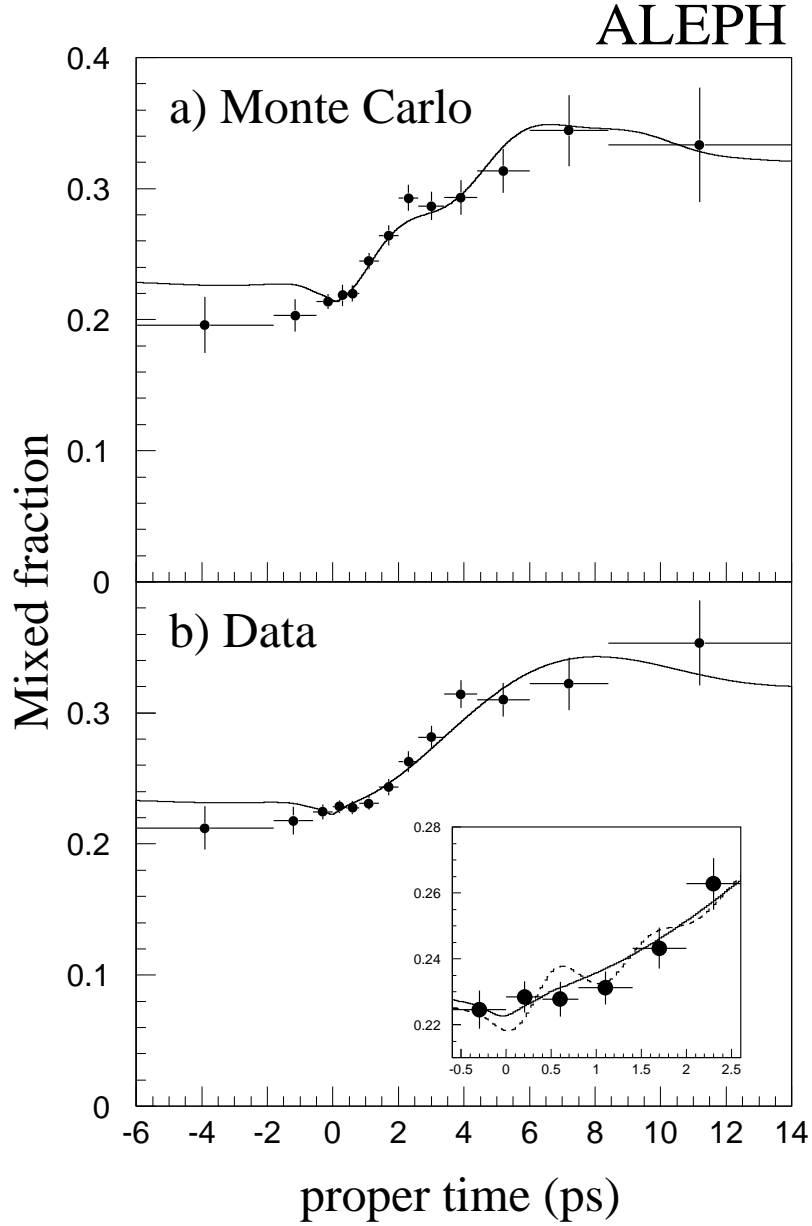
14

Figure 6: The tagged mixed fraction of events as a function of measured proper time, for a) Monte Carlo with $\Delta m_s = 1.6$ ps^{-1}, and b) data events. The superimposed curve for the Monte Carlo in a) is the expected distribution for $\Delta m_s = 1.6$ ps^{-1}. The solid curve for the data in b) assumes $\Delta m_s = 30$ ps^{-1}, while the dashed curve in the insert is the expected distribution for $\Delta m_s = 6$ ps^{-1}. The small proper time region of the plot is expanded to emphasize the part most sensitive to B_s^0 oscillations.
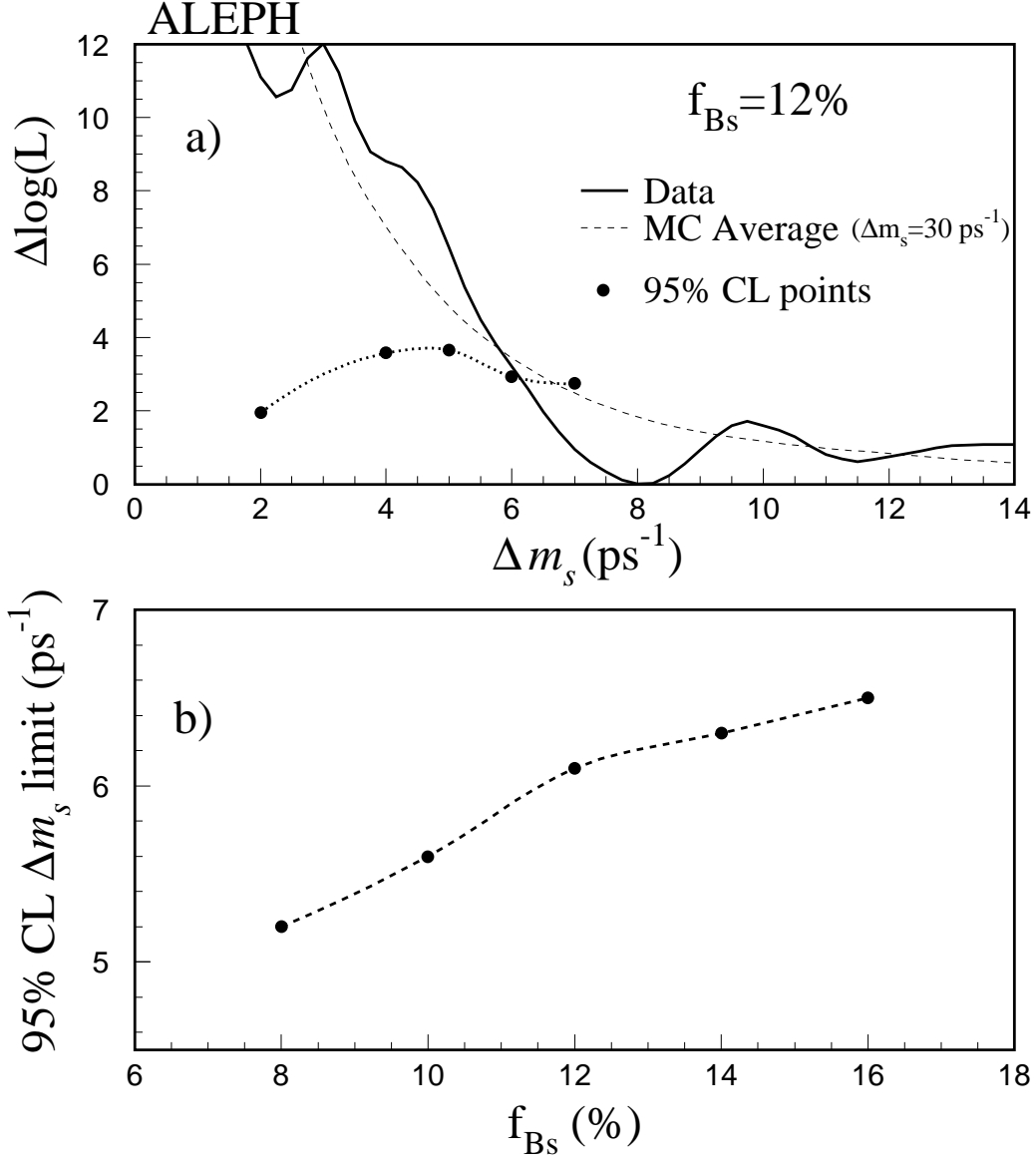
Figure 7: a) Superimposed on the data likelihood curve are the average of the fast Monte Carlo $\Delta \log L$ values, and the 95% confidence limit points. $\Delta \log L$ is defined as the $-\log L$ value at the Δm_s value, minus the minimum $-\log L$ value. A limit curve is drawn through the 95% confidence limit points. The data curve crosses the limit curve at $\Delta m_s = 6.1$ ps^{-1} for B_s^0 fraction $f_{B_s} = 12\%$. Also shown is the average of the $\Delta \log L$ curves for 200 fast Monte Carlo samples in which B_s^0 mixing is near-maximal ($\Delta m_s = 30$ ps^{-1}). b) The results of 95% confidence level limit in Δm_s as a function of the B_s^0 fraction f_{B_s}. The limits for Δm_s are 5.2, 5.6, 6.1, 6.3 and 6.5 for $f_{B_s} = 8\%$, 10%, 12%, 14% and 16%, respectively.

16

parameter	value		error
A_u $(B_s^0 \to \ell)$	0.817	$\pm$	0.010
A_u $(B_d^0 \to \ell)$	0.831	$\pm$	0.004
A_u (other $b \to \ell$)	0.874	$\pm$	0.003
A_m $(B_s^0 \to \ell)$	0.722	$\pm$	0.014
A_m $(B_d^0 \to \ell)$	0.624	$\pm$	0.015
A_u $(B_s^0 \to c \to \ell)$	0.238	$\pm$	0.036
A_u $(B_d^0 \to c \to \ell)$	0.309	$\pm$	0.014
A_u (other $b \to c \to \ell$)	0.247	$\pm$	0.012
A_m $(B_s^0 \to c \to \ell)$	0.075	$\pm$	0.027
A_m $(B_d^0 \to c \to \ell)$	0.193	$\pm$	0.027
$A_{c\bar{c}}$	0.846	$\pm$	0.007
A_{uds}	0.633	$\pm$	0.016

Table 4: Input tag rates in the fast Monte Carlo. The listed errors are due to statistical fluctuations in the generation of event samples which correspond to the size of the ALEPH data sample.

parameter	value		uncertainty
τ_b (ps)	1.54	$\pm$	0.05
τ_{B_s} (ps)	1.5	$\pm$	0.2
Δm_d (ps^{-1})	0.50	$\pm$	0.05
f_{Λ_b}	0.10	$\pm$	0.04
$f_{B_s}^{bc}$	0.088	$\pm$	0.009
$f_{B_d}^{bc}$	0.140	$\pm$	0.014
$f_{other\,b}^{bc}$	0.100	$\pm$	0.010
f_{uds}	0.05	$\pm$	0.02
$f_{c\bar{c}}$	0.09	$\pm$	0.02
f_{sb}	0.025	$\pm$	0.025
A_u $(B_s^0 \to \ell)$	0.817	$\pm$	0.080
A_m $(B_s^0 \to \ell)$	0.722	$\pm$	0.030
$A_{c\bar{c}}$	0.846	$\pm$	0.080
A_{uds}	0.633	$\pm$	0.020
S_{res}	1.10	$\pm$	0.10

Table 5: Parameter uncertainties input to the fast Monte Carlo. Data sets are generated with the listed parameters selected in Gaussian distributions around their central values with widths given by the indicated uncertainties.

later.) The b baryon fraction f_{Λ_b} is selected randomly using the central value and width indicated in Table 5. The value of $f_{B_d} = f_{B^+}$ is then determined by the constraint: $f_{B_s} + f_{\Lambda_b} + f_{B_d} + f_{B^+} = 1$.

The fractions f_{B_d} and f_{B_s} are adjusted for the relative reconstruction efficiencies $\mathcal{E}_{B_d}$ and $\mathcal{E}_{B_s}$ of these mesons compared to the non-oscillating b hadrons ($B^{\pm}$ mesons and b baryons). The fractions $f_{B_s}^{bc}$, $f_{B_d}^{bc}$, and $f_{other\,b}^{bc}$ are used to generate the respective fractions of cascade leptons for the B_s^0 and B_d^0 mesons and other b hadrons.

A true momentum and decay length are generated for each $b\bar{b}$ event. The true momentum is generated according to the true momentum distribution of b hadrons (taken from the fully simulated Monte Carlo after the final event selection), and the true decay length is calculated using the true momentum and a true proper time generated using an exponential decay-time distribution. The generated input τ_b is varied by the indicated error. Proper-time dependent efficiencies are included, which redistribute the proper times slightly. The decay length and momentum resolutions vary as functions of true decay length and true momentum respectively, and the reconstructed values are smeared accordingly, using eight slices in decay length and seven in momentum. The fast Monte Carlo resolution is degraded by a factor $S_{res} = 1.10 \pm 0.10$ relative to the resolution found in the fully simulated Monte Carlo (see Section 3). The class of b events (see Section 6) where the decay length is reconstructed near the primary vertex independent of the true b decay length are also included in the fast Monte Carlo.

The true proper time and momentum generation is done the same way for cascade decays ($b \to c \to \ell$) as for normal $b \to \ell$ decays. The slightly longer reconstructed decay length from the subsequent c decay is simulated using a resolution parameterization with a positive shifted mean. For B_s^0 and B_d^0 mesons, the true proper decay time is used to determine the true mixed/unmixed state. The probability that an event is tagged as mixed or unmixed is then generated based on the lepton signed jet charge tag rates of each species of b hadron in the fully simulated Monte Carlo (A_m and A_u for mixed and unmixed, respectively), according to whether the lepton comes from a direct semileptonic b hadron decay, or a subsequent cascade decay. These values of A_m and A_u are listed in Table 4. Since the average value of A_u was fit from the data with an error of 0.003, and there is agreement between data and Monte Carlo to that level, the individual values for unmixed tag rates A_u for the different event sources are fixed so that the average is constrained, and the uncertainty in the average is simulated by choosing the unmixed tag rate for $B_s^0 \to \ell$ events from a Gaussian distribution with σ large enough to cover the uncertainty in the average unmixed tag rate. The uncertainty in A_u for $B_s^0 \to \ell$ events is thus set at 0.08. The uncertainty in A_m for $B_s^0 \to \ell$ events is set at 0.03 using the same procedure.

The charm and uds contributions are simulated in a slightly different way. The reconstructed decay length and momentum distributions, also from the fully simulated Monte Carlo (after final selection), are used to generate events. The fraction of these events which are tagged unmixed is taken from the fully simulated Monte Carlo. These fractions

are $A_{c\bar{c}}$ and A_{uds}, respectively.

The likelihood differences $\Delta \log L$ for the fast Monte Carlo are then calculated for 300 samples at various input values of Δm_s (2.0, 4.0, 5.0, 6.0, and 7.0 ps^{-1}), each with sample size equal to that of the data. (600 samples are used if the Δm_s value is close to where the limit is set.) The 95% confidence limit is determined by locating the point below which lie 95% of the $\Delta \log L$ values, calculated at the input value of Δm_s. The 95% confidence limit curve is then drawn through the points at different input Δm_s, as shown in Fig 7(a). The data $\Delta \log L$ curve intersects the limit curve at $\Delta m_s = 6.1$ ps^{-1}. This is taken as the 95% confidence level lower limit.[2]

A limit of $\Delta m_s = 6.0$ ps^{-1} is obtained if the likelihood difference $\Delta \log L$ is defined instead as the $-\log L$ value at a given Δm_s minus the $-\log L$ value calculated at near–maximal mixing ($\Delta m_s = 30$ ps^{-1}).

As the B_s^0 meson fraction f_{B_s} is not accurately known, and plays a special role on the sensitivity of the analysis to oscillations, the systematic effect of this parameter is studied by repeating the fast Monte Carlo experiments using different values of f_{B_s} as inputs. The corresponding input value is also input into the fitting function for both the data and fast Monte Carlo samples. Fig 7(b) shows the results of 95% confidence level lower limit in Δm_s as a function of f_{B_s}. The limit varies from $\Delta m_s > 5.2$ ps^{-1} at $f_{B_s} = 8\%$ to $\Delta m_s > 6.5$ ps^{-1} at $f_{B_s} = 16\%$. Values[3] of $f_{B_s} = (13 \pm 3)\%$ and $f_{B_s} = (12.2 \pm 3.2)\%$ have been estimated elsewhere [11, 22].

To check that the data curve is consistent with a Δm_s value larger than the limit value, 200 fast Monte Carlo samples with equivalent statistics to the ALEPH data sample were generated with $f_{B_s} = 12\%$ and $\Delta m_s = 30$ ps^{-1} (near–maximal mixing). In 50% of the samples, the simulated likelihood curve crosses the 95% CL limit curve at a Δm_s value greater than 6.1 ps^{-1}. This demonstrates that the limit set with the ALEPH data is within the sensitivity expected from Monte Carlo studies.

8 Conclusions

A lower limit has been set for the B_s^0 oscillation parameter using a jet charge technique and an unbinned maximum likelihood fitting function, by comparing the ALEPH data to expected distributions generated with a fast Monte Carlo simulation. Varying the fraction f_{B_s} of b quarks from Z^0 decays that form B_s^0 mesons from 8% to 16%, the 95% confidence level lower limit of Δm_s ranges from 5.2 to 6.5 ps^{-1}. Taking $f_{B_s} = 12\%$, as

---

[2]The equivalent lower limits in Δm_s are 5.0 and 5.8 ps^{-1} for the 1991 to 1993 data, and the 1994 data respectively, the two data samples being roughly equal in statistics. This result supercedes the preliminary result using the 1991 to 1993 data reported in the 1994 Glasgow Conference.

[3]Strictly speaking, this is the production fraction without weighting by the ratio of the B_s^0 semileptonic branching fraction to the average semileptonic branching fraction; the difference of the B_s^0 semileptonic branching fraction and the average is, however, expected to be small.

favored by other analyses [11, 22], a lower limit of $\Delta m_s > 6.1$ ps^{-1} is set at 95% confidence level. The limit value corresponds to 4.0×10^{-3} eV. Since $x_s = \Delta m_s \, \tau_{B_s}$, this limit also gives $x_s > 8.8$, using the B_s^0 lifetime of $\tau_{B_s} = 1.55 \pm 0.11$ ps [21, 23] and shifting the central value of τ_{B_s} down by 1σ. Using the world average central values [5, 20] of the quantities in equation 3, and including their uncertainties by shifting the values by 1σ to the conservative side, yields $|V_{ts}/V_{td}| > 2.6$ for $f_{B_s} = 12\%$. Varying f_{B_s}, $|V_{ts}/V_{td}| > 2.4$ for $f_{B_s} = 8\%$, and $|V_{ts}/V_{td}| > 2.7$ for $f_{B_s} = 16\%$.

Acknowledgements

References

[1] E. Paschos and U. Türke, Phys. Rep. **178** (1989) 145.

[2] N. Cabibbo, Phys. Rev. Lett. **10** (1963) 531; M. Kobayashi and T. Maskawa, Prog. Theor. Phys. **49** (1973) 652.

[3] J. Shigemitsu, Proc. XXVII Int. Conf. on HEP, Glasgow, Scotland (1994) Vol I 135.

[4] S. Narison, Phys. Lett. **B 322** (1994) 247; S. Narison and A. Pivovarov, Phys. Lett. **B 327** (1994) 341.

[5] A. Ali and D. London, Z. Phys. **C 65** (1995) 431.

[6] D. Buskulic *et al.* (ALEPH Collab.), Phys. Lett. B **313** (1993) 498.

[7] D. Buskulic *et al.* (ALEPH Collab.), Phys. Lett. **B 322** (1994) 441.

[8] R. Akers *et al.* (OPAL Collab.), Phys. Lett. **B 327** (1994) 411.

[9] R. Akers *et al.* (OPAL Collab.), Phys. Lett. **B 336** (1994) 585.

[10] P. Abreu *et al.* (DELPHI Collab.), Phys. Lett. **B 338** (1994) 409.

[11] R. Akers *et al.* (OPAL Collab.), *A Study of B Meson Oscillations Using Dilepton Events*, CERN-PPE/95-12, (January 1995), submitted to Z. Phys. C.

[12] W. Ash *et al.*, Phys. Rev. Lett. **58** (1987) 1080.

[13] D. Decamp *et al.* (ALEPH Collab.), Nucl. Inst. Methods **A 294** (1990) 121.

[14] D. Buskulic *et al.* (ALEPH Collab.), *Performance of the ALEPH Detector at LEP*, CERN–PPE/94–170, (November, 1994), to be published in Nucl. Inst. Methods.

[15] T. Sjöstrand and M. Bengtsson, Computer Phys. Commun. **43** (1987) 367.

[16] J. Körner and G. Schuler, Z. Phys. **C 38** (1988) 511.

[17] S. Bethke *et al.* (JADE Collab.), Phys. Lett. **B 213** (1988) 235.

[18] D. Buskulic *et al.* (ALEPH Collab.), Nucl. Inst. Methods **A 346** (1994) 461.

[19] C. Peterson *et al.*, Phys. Rev. **D 27** (1983) 105.

[20] L. Montanet *et al.* (Particle Data Group) Phys. Rev. **D 50** (1994) 1173.

[21] M. Jimack, *b-physics at LEP*, Proc. of XXX Rencontres De Moriond (Les Arcs, Savoie, France), March, 1995.

[22] D. Buskulic *et al.* (ALEPH Collab.), *A Measurement of $|V_{cb}|$ from $\overline{B}^0 \to D^{*+}\ell^-\bar{\nu}_\ell$*, in preparation.

[23] F. Abe *et al.* (CDF Collab.), *Measurement of the B_s Meson Lifetime*, FERMILAB–PUB–94/420–E, (December, 1994), to be published in Phys. Rev. Letters.